RSC Advances

ROYAL SOCIETY OF CHEMISTRY

www.rsc.org/advances

Ultrasensitive an amperometric environmental toxic hydrazine sensor of reduced graphene oxide/gold tetraphenyl porphyrin (RGO/Au-TPP) nanocomposite

Subramanian Sakthinathan[a], Subbiramaniyan Kubendhiran[a], Shen-Ming Chen[a]*, P.Tamizhdurai[b]

[a]*Electroanalysis and Bioelectrochemistry Lab, Department of Chemical Engineering and Biotechnology, National Taipei University of Technology, No.1, Section 3, Chung-Hsiao East Road, Taipei 106, Taiwan (R.O.C).*

[b]*National Centre For Catalysis Research, Indian Institute of Technology, Chennai, India.*

[*]*Corresponding Author (S.M. Chen). Fax: +886 2270 25238; Tel: +886 2270 17147,*

E-mail: smchen78@ms15.hinet.net

Abstract

Gold tetra phenyl porphyrin / reduced graphene oxide (RGO/Au-TPP) nanocomposite film modified glassy carbon electrode (GCE) was prepared for the trace level detection of hydrazine. The prepared nanocomposite was characterized by scanning electron microscope, X-ray diffraction studies, Transmission electron microscope, Ultraviolet-visible spectroscopy, Infrared spectroscopy and Raman spectroscopy. The electrochemical studies of the modified electrode was carried out by the Cyclic voltammetry and Amperometric (*i*-*t*) method. The RGO/Au-TPP/GCE exhibits enhanced electrocatalytic activity towards detection of hydrazine. The detection limit is 3 nM, the linear range is between 20 nM and 198 μM L^{-1}, and the sensitivity is 2.266 μA μM^{-1} cm^{-2}. Besides, the modified electrode selectively detects hydrazine in presence of 500 fold excess concentrations of other interfering ions. The practical applicability of the sensor has been addressed in ground water samples which shows satisfactory recoveries. Moreover, the sensor has shown acceptable repeatability, reproducibility and higher stability.

Keywords

Reduced graphene oxide, Gold tetra phenyl porphyrin, Hydrazine, Sensor, Electrocatalysis, Amperometry, Selectivity, Real sample analysis.

1.Introduction

Hydrazine and its derivatives are widely used in the industrial, pharmaceutical and agricultural applications.[1-5] Despite their excellent applications, they are highly toxic to human beings and animals. They can easily absorbed by oral, skin and breathing routes and affects luncks, liver, kidney and central nervous system of living organisms and make mutagenic effect.[6-8] The World Health Organization (WHO) and the environmental protection agency (EPA) USA were classified hydrazine as B2 group human carcinogens.[9] Therefore, sensitive and selective detection of hydrazine is highly important.[10,11] Different analytical methods have been used for the detection of hydrazine such as, gas chromatography-mass spectrometry (GC-MS),[12] spectro photometric methods[13], flow injection analysis,[14] potentiometry method,[15] high performance liquid chromatography (HPLC)[16] and titrimetry analysis.[17] Although, these traditional methods are sensitive to detect hydrazine, they involve high cost, laborious, require specially tranined professional, and involve tedious protocols. The electrochemical techniques are better alternative due to their low-cost, fast response, simple and portable.[18] However, the unmodified electrodes exhibit high overpotential, low sensitivity and electrode fouling in hydrazine sensing. The modified electrodes are more prefereable to circumvent the issues encountered by bare electrodes. In recent years, carbon nano materials such as, graphite,[19] carbon nanotubes (CNTs),[20] graphene,[21] and activated carbon[22] have been widely employed in electrochemical sensor applications.

Graphene received enormous interest in various fields of research due to its large surface area, excellent electrical conductivity, thermal conductivity, higher mechanical strength and ease of functionalization.[23,24] Graphene based nanocomposites were successfully employed in supercapacitors,[25] batteries,[26, 27] sensor,[28] drug delivery,[29] solar cells[30] and catalysis.[31] The oxidation of graphite with subsequent reduction of graphene oxide is the most widely employed approach to prepare graphene based composites. Generally, three major reduction methods such as, thermal,[32] chemical,[33] and electrochemical methods were known for graphene oxide reduciton.[34] Eventhough, the thermal and chemical reduction required high temperature, high vacuum and toxic chemicals. Compared with thermal and chemical methods, the electrochemical methods are simple, fast, efficient, low-cost, and environmentally friendly. In addition, it is easy to control film thickness and formation of stable films without any other modification.[35]

Porphyrin, a conjugated organic macromolecule coordinate with metal ion to form stable metal tetra phenyl porphyrin. The metal porphyrins are good electrocatalysts towards oxidation and reduction of several important small molecules and biologically important analytes.[36-38] In the literature, metal porphyrins are proved as effective electrocatalysts for the oxidation of hydrazine.[39,40] Graphene have been used as an extensive substrate material for different porphyrin derivatives assembly on the electrode. Gold tetraphenyl porphyrin (Au-TPP) as a multidentate ligand and it has an excellent electron acceptor and electron donor ability.[41-43]

In the present work, Au-TPP complex was assembled on the reduced graphene oxide surface through non-covalent π-π stacking interaction using eco-friendly route. The conjugation between metal porphyrin and graphene oxide was greately increased after nanocomposite formation. The preparation method used here is simple, efficient, toxic-free and does not involve high temperature or tedious protocols. The RGO/Au-TPP nanocomposite exhibit excellent electrocatalytic abilty to oxidize hydrazine and delivered significantly improved electrocatalytic parameters including low detection limit and wide linear range.

2. Experimental

2.1 Reagents

Graphite (powder 1-2 μm), benzaldehyde, pyrrole, propionic acid, chloroform, methanol, chloroauric acid ($HAuCl_4\ _3H_2O$), potassium ferro cyanide, sodium acetate, acetic acid, potassium ferric cyanide, uric acid, ascorbic acid and all other chemicals received from Sigma-Aldrich. Sulfuric acid (H_2SO_4) and hydrochloric acid (HCl) was purchased from Merck Chemical. Hydrazine monohydrate was purchased from Alfa Aesar. The supporting electrolyte was phosphate buffer solution (PBS) (pH 7) which was prepared by using Na_2HPO_4 (0.05 mol L^{-1}) and NaH_2PO_4 (0.05 mol L^{-1}). Double distilled water (the conductivity is 0.05 μS/cm) was used to prepare all solutions. A stock solution of hydrazine was prepared by PBS (pH 7) and the electrolyte was deoxygenated by purging nitrogen.

2.2 Experimental apparatus

Electrochemical measurements were carried out using CHI 410 and CHI 750a electrochemical work stations (Shanghai Chen Hua. Co). Three electrode system consists of

glassy carbon electrode (area = 0.07 cm^2) as working electrode, saturated Ag/AgCl (KCl) as reference electrode and platinum wire as an auxiliary electrode was used. Amperometric measurements were performed using analytical rotator AFMSRX (PINE instruments, USA) and rotating disc glassy carbon electrode (RDE, area = 0.21 cm^2). ^1H NMR spectroscopy was recorded in JEOL 500 MHz and UV–Visible spectra were recorded in JASCO V770, respectively. The morphological structure of the sample was characterized by SEM measurements with a Hitachi S-3000 H, and the elemental analysis carried out from HORIBA EMAX X-ACT (model 51-ADD0009) instrument. TEM investigations were performed using JEOL 2000 transmission electron microscope (operating at 200 kv), wherein the sample were dripped on standard carbon/Cu grids and used for the TEM analysis. Electrochemical impedance spectra (EIS) were carried out using ZAHNER (Kroanch, Germany) impedance analyser. X-ray diffraction (XRD) patterns were obtained from XPERT-PRO diffraction meter using CuK radiation (k = 1.54 A) operating 40 KV and 20 mA. Perkin-Elmer IR spectrometry used for the IR studies. The Raman spectra were recorded on a Jobin Yvon T64000 Spectrometer equipped with a charge coupled device (CCD) detector cooled with liquid nitrogen. The back scattering signal was collected with a microscope using an Ar^+ laser centered at 488 nm as the excitation source. The thermal properties of composites were determined by TGA with a PL Thermal Sciences (model PL-STA) using a heating rate of 10 ◦C/min from room temperature to 800º C under N_2. Moreover, all the electrochemical experiment was carried out at ambient temperature.

2.3 Preparation of gold tetra phenyl porphyrin (Au-TPP)

The Au-TPP was prepared by according to the previous report with slight modification.[44-46] The prepared reaction mixture was washed with water to remove excess of reactant materials. Finally, the solvent was dried by rotatory evaporator after that removal of solvent was chromatographed on a silica gel column packed with $CHCl_3$ (Scheme 1). The final nanocomposite was characterized and confirmed by ^1H NMR (Fig. S1, S2) and UV-Visible spectroscopies and then stored in refrigerator.

2.4 Preparation of reduced graphene oxide/Au-tetraphenyl porphyrin (RGO/Au-TPP) nanocomposite

The Scheme 2 shows the preparation of RGO/Au-TPP nanocomposite. Graphene oxide (GO) was prepared from the graphite by modified Hummer's method.[47] It is formed through π-π stacking interaction between the graphene oxide and Au-TPP. In brief, the prepared Au-TPP suspension was dropped (5 μL) into the graphene oxide (0.5 mg/ml^{-1}) and it was sonicated for 20 min. After the sonication process, GO/Au-TPP (8 μL) (Fig. S3) solution was dropcasted on the GCE surface and at room temperature. Next, the GO/Au-TPP/GCE was transferred into an electrochemical cell containing 0.05 M acetate buffer. Cyclic voltammograms were carried out by applied potential of 0 V to –1.4 V (Fig. S4). Then, the prepared RGO/Au-TPP nano composite modified electrode was used for the hydrazine sensor.

3. Results and discussion

3.1 Characterization of prepared nano composite

The surface morphological studies and differences in exfoliation behaviour were clearly examined by SEM. Fig. 1 shows the morphological structure of (A) GO, (B) RGO, (C) GO/Au-TPP, (C') Au-TPP and (D) RGO/Au-TPP. The SEM image of GO (Fig. 1A) depicts a stacked multilayer and thin curtain like morphology. The RGO (Fig 1 B) shows portrays thin and wrinkled sheet structure. The Fig. 1C shows the GO/Au-TPP structure, it clearly exhibits that the Au-TPP complex incorporation with the GO sheet. The RGO/Au-TPP nanocomposite (Fig. 1D) shows the Au-TPP complex was uniformly distributed and regular decoration on the graphene oxide surface. Fig. 1E exhibits the EDX spectrum of RGO/Au-TPP nanocomposite with weight percentage C (59.05 %), N (21.21 %), O (6.63 %) and Au (13.11 %) respectively. The weight percentage (Fig. 1F) proof that the successfully formation of RGO/Au-TPP nanocomposite. Fig. 2 shows the TEM images of RGO (A), Au-TPP (B) and RGO/Au-TPP nanocomposite (C), (D). Fig 2A exhibited that the RGO, it has wrinkled and folding sheet structure. Fig. 2B shows the aggregated structure of Au-TPP complex. The TEM image of Fig. 2C and 2D shows the RGO/Au-TPP nanocomposite, it demonstrate that the Au-TPP complex was randomly incorporated on the reduced graphene oxide surface.

Raman spectroscopy is widely used to characterize the crystal structure and disorder of graphene based materials. [48] Fig. 3A shows the Raman spectra of (a) Au-TPP, (b) RGO, (c) RGO/Au-TPP nanocomposite. The Raman spectrum of Au–TPP exhibited, the aromatic

stretching vibrations are observed at 1454 and 1528 cm^{-1} and the stretching vibrations of pyrrole ring on the porphyrin at 1348 and 1392 cm^{-1}. In addition, the Au–TPP complex featured with C–H and C=C vibrations at 1247 cm^{-1} and 1068 cm^{-1}, respectively which is in good agreement with the previous reports.[49] Moreover, the Raman spectrum of RGO exhibits the D and G bands at 1335 cm^{-1} and 1590 cm^{-1}, respectively. The D and G bands of RGO/Au-TPP nanocomposite shifted to 1359 and 1602 cm^{-1}, which indicates that the possible interaction between RGO and Au-TPP complex. The FT-IR spectroscopy is an effective method to identify the graphene functionalization.[50] Fig. 3B presents the FT-IR spectra of (a) RGO, (b) Au-TPP and (c) RGO/Au-TPP nanocomposite. The RGO exhibits the O–H stretching vibration at 3500 cm^{-1} and the stretching vibrations of C=O and C–O were observed at 1730 cm^{-1} and 1050 cm^{-1}, respectively. The FT–IR spectrum of Au–TPP shows the N–H vibrations at 3400 cm^{-1} and C-H stretching at 2925 cm^{-1}. Moreover, the bands at 1496 cm^{-1} and 1334 cm^{-1} were assigned to the C=C and C=N stretching vibration. When the Au–TPP complex immobilized on RGO, the C=C and C=N bands of RGO/Au–TPP nanocomposite were shifted to 1770 cm^{-1} and 1250 cm^{-1} respectively. It can be attributed to the strong π-π interaction between the Au-TPP and RGO.

Fig. 4A shows the UV-Visible spectra of (a') GO, (b') RGO, (c) TPP, (d) Au-TPP and (d) RGO/Au-TPP. The metallated tetra phenyl porphyrin dissolved in distilled chloroform and the UV-visible spectra are taken at room temperature. The UV-Vis spectra of GO and RGO show absorbance at 220 nm and 283 nm respectively. Moreover, the TPP complex have the absorption peak of soret and weaker (Q) bands at 420 nm and 512, 550, 553 nm, respectively. In addition, the Au-TPP complex exhibit the soret and Q bond at 416 and 511, 542, 548, respectively. The absorbance values of Au–TPP complex has been decreased in comparison with TPP absorbance which indicated the possible interaction between Au and TPP complex. Moreover, the RGO/Au-TPP nanocomposite shows the absorbance of soret and Q bands at 412 and 508, 541 nm respectively. The RGO/Au-TPP nanocomposite absorbance values are changed from RGO and Au-TPP absorbance due to the red shifting and it is good evidence for noncovelent non-covalent π-π stacking interaction.

Electrochemical impedance spectroscopy is an efficient tool to analyze the electron transfer between the electrolyte and the electrode surface. Fig. 4B shows the Nyquist plot (–Z'' vs Z') of (a) bare GCE, (b) GCE/GO, (c) GCE/Au-TPP, (d) GCE/RGO and (e) GCE/RGO/Au-TPP

modified electrodes in 5 mM $[FeCN_6]^{3-}$ / $[FeCN_6]^{4-}$ solution containing 0.05 M PBS of pH 7 with supporting electrolyte 0.1 M KCl. The frequency range between 100 mHz and 100 KHz was applied for EIS analysis. The charge transfer resistance (R_{ct}) value of each modified electrode can be identified by fitting the Nyquist plot with the Randles equivalent circuit model. The bare GCE displayed a large semicircle with R_{ct} of 906 Ω, it is attributed to the poor conductivity. After that, the GCE/Au-TPP and GCE/GO modified electrode shows the *Rct* values, 897 Ω and 588 Ω respectively. The GCE/RGO modified electrode shows the small semicircle with R_{ct} of 207 Ω. Finally, the RGO/Au-TPP nanocomposite film modified electrode shows the lowest R_{ct} of 168 Ω which is due to the less electrode resistance. In other words, the low resistance of the electrode should be ascribed to the high electronic conductivity of the nanocomposite.

Thermal stabilities of (a) RGO, (b) Au-TPP and (c) RGO/Au-TPP nanocomposite were examined by thermogravimetric analysis (TGA) under N_2 atmosphere at heating rate 10°C/min (Fig S5). The RGO is thermally stable up to 300°C and the weight loss of 10% ascribed to the absorbed water. Then, the 20% weight loss between 300 to 600°C was attributed to the oxygen containing functional groups. Moreover, the stability of RGO was higher with only 5% weight loss up to 800°C. The Au-TPP complex was thermally stable up to 380°C due to the existence of conjugated structure and the weight loss occurred till 380°C. The RGO/Au-TPP retained about 60 % of the original mass up to 800°C. Thus, TGA results indicating that the stability of the Au-TPP complex is signifantly improved after its incorporation with RGO as composite.

4. Electrocatalytic oxidation of hydrazine

4.1 Electro oxidation of hydrazine at various modified electrodes and different scan rate

Fig. 5A exhibits that the electrocatalytic oxidation of hydrazine at different modified electrodes such as (a) bare GCE, (b) GO, (d) RGO, (e) Au-TPP, (f) GO/Au-TPP and (g) RGO/Au-TPP nanocomposite modified electrodes in PBS (pH 7) containing 200 μM hydrazine at the scan rate 50 mVs^{-1}. The CVs of (C) RGO/Au-TPP nanocomposite modified electrode shows the absence of hydrazine at the scan rate 50 mVs^{-1}. The CVs of bare GCE and GO have not shown significant hydrazine oxidation. The RGO exhibited enhanced background current, but there is no obvious peak appeared for hydrazine oxidation. However, the Au-TPP modified electrodes show oxidation peaks (E_p) at 0.16 V, and peak currents (I_p) at 43.85 μA (Fig S8).

Inaddition, the GO/Au-TPP modified electrode exhibit the hydrazine oxidation peak (E_p) at 0.2 V and peak current (I_p) at 63.75 μA. The RGO/Au-TPP nanocomposite modified electrode there is no peak appeared without the addition of hydrazine. Interestingly, addition of 200 μM hydrazine, the RGO/Au-TPP nanocomposite exhibited sharp oxidation peak at E_p of 0.18 V with I_p of 87.93 μA in presence of 200 μM hydrazine. Undoubtedly, the RGO/Au-TPP nanocomposite act as a best electrode material for the electrocatalytic oxidation of hydrazine than previously reported carbon based electrodes (Table 1). Fig. 5B shows the cyclic voltammograms of RGO/Au-TPP nanocomposite modified electrode in 0.05 M PBS (pH 7) with increasing the concentration of hydrazine form 50 μM to 600 μM (a–k). The oxidation peak current increases linearly with increasing the concentration of hydrazine which indicate the modified electrode act as an efficient electrode material for the electrocatalytic oxidation of hydrazine. The inset of Fig. 5B shows the plot of peak current vs concentration of hydrazine and the plot exhibits linear relationship. Besides, the slope value nearly equal to 1 which indicates that the electrocatalytic oxidation follows first order kinetic reaction.

4.2. Effect of pH and different scan rate on oxidation of hydrazine

Fig. 6A shows the electrocatalytic oxidation of hydrazine (200 μM) at the RGO/Au-TPP nanocomposite modified electrode in different pH, from 3 to 11. The pH studies revealed that the hydrazine oxidation peak current was not affected by varying pH, however the peak potential (Ep) shifted from positive to negative side as the pH increases. The RGO/Au-TPP nanocomposite has the higher oxidized peak current for hydrazine at pH 7 and hence we have chosen pH 7 as the optimum pH for all the experiments (Fig. 6C). The Fig. 6B shows the linear relation between pHs and E_p and the slope value of 59 mV/pH. The obtained slope value is close to the theoretical Nernst equation which indicates that an equal number of protons and electron transfer in the oxidation of hydrazine[51].

Fig. 7A shows the effect of scan rate on the RGO/Au-TPP nanocomposite film modified electrode in presence of 200 μM hydrazine in PBS (pH 7). The oxidation peak current is linearly increased as the scan rate increases. Moreover, the anodic peak potential shifted to a positive value (20 to 200 mVs^{-1}). The Fig. 7B shows the oxidation peak current of hydrazine was linear against the square root of scan rate, with a correlation coefficient of 0.995 and which indicates that the hydrazine oxidation at RGO/Au-TPP nanocomposite modified GCE electrode as a

diffusion controlled reaction. In addition, the corresponding linear regression equation can be expressed us I_p (μA) = 700.21 $v^{1/2}$ $(Vs^{-1})^{1/2}$ + 88.407, R^2 = 0.995. On the other hand, the plot of anodic peak potential (E_{pa}) vs logarithm of scan rate (log v) exhibit the linear relationship, the corresponding linear regression equation can be expressed as E_{pa} (V)= 0.1156 log v (Vs^{-1}) + 0.4074, R^2 = 0.9952. Therefore, the oxidation of hydrazine at the RGO/Au-TPP nanocomposite modified electrode is an electrochemical irreversible process, it can be expressed as.[52]

$$E_{pa}=[\ 2.303RT/(1-\alpha)\ n_aF\ ]\ log\gamma + K \qquad (1)$$

Here, R, T and F as the constant value (R= 8. 314 JK mol^{-1}, T= 298 K and F= 96485 C mol^{-1}), α is the electron transfer coefficient, n_a is the number of electron involved in the rate determining step and K is the constant. Here, the slope value 115.6 mV is close to the theoretical value, it is indicating that one electron transfer was involved in the rate determining step. Furthermore, the number of electrons involved in the overall reaction is calculated by below eq. 2.[53]

$$Ip = (2.99 \times 10^5)\ n\ [(1-\alpha)n_a]^{1/2}\ AC_oD_o^{1/2}\gamma^{1/2} \qquad (2)$$

Here, A is the electrode area, D_o is the diffusion coefficient and C_o is the bulk concentration of hydrazine. By substituting all the values in the eq. (2), the value of n is estimated to be 4. Therefore, the oxidation of hydrazine at RGO/Au-TPP nanocomposite involves four electron transfer and their following mechanisms can be expressed as 3-5.[5]

$$AuTPP–Au\ (III) + N_2H_4 + H_2O \rightarrow AuTPP–Au\ (II) + N_2H_3 + H_3O^+ + e^- \quad (slow) \qquad (3)$$

$$AuTPP–Au\ (III) + N_2H_3 + 4H_2O \rightarrow AuTPP–Au\ (II) + N_2 + 4H_3O^+ + 4e^- \quad (fast) \qquad (4)$$

$$AuTPP–Au\ (III) + N_2H_4 + 4H_2O \rightarrow AuTPP–Au\ (II) + N_2 + 4H_3O^+ + 4e^- \quad (overall\ reaction) \qquad (5)$$

Hence the oxidation of hydrazine at RGO/Au-TPP nanocomposite modified electrode can be expressed by equation.

4.3. Amperometric determination of hydrazine

Fig. 8A shows the amperometric response of RGO/Au–TPP nanocomposite modified rotating disc electrode upon each successive addition of hydrazine into continuously stirred PBS at the rotation speed 2500 RPM and applied potential 0.16 V. The sensor exhibited quick

amperometric response towards each sequential addition of hydrazine. The proposed sensor reaches its 95% steady-state current within 2 sec which revealed fast electrocatalysis. Fig. 8B shows the linear regression equation and the corresponding linear regression equation was expressed as I_p (A) = 0.476 [hydrazine] (μM) + 4.095. The sensitivity was estimated to be 2.266 μA μM cm^2. The amperometric response of hydrazine in the linear range from 20 nM to 198 μM L^{-1} and the limit of detection is calculated to be 3 nM (LOD = 3 S_b/S, S_b indicates the standard deviation of the blank signal and S indicates the sensitivity). The proposed sensor exhibited comparable performances with other modified electrode. Notably, the prepared sensor achieved LOD of 3 nM which is comparatively lower than the other reported modified electrodes. Undoubtedly, the RGO/Au-TPP nanocomposite modified electrode exhibit the outstanding electrocatalytic activity towards the lowest detection of hydrazine.

4.4 Interference and real sample analysis

The selectivity of the RGO/Au-TPP nanocomposite towards the determination of hydrazine (a) in presence of common interfering ions, such as, Na^+ (b), K^+ (c), Ca^+ (d), Mg^{2+} (e), Cu^{2+} (f), F^- (g), Cl^- (h), Br^- (i), I^- (j), NO_3^- (k), dopamine (l), glucose (m), fructose (n), lactose (o), arginine (p) and ascorbic acid (q) were investigated (Fig. 9A). The RGO/Au-TPP nanocomposite exhibited good response towards hydrazine addition. However, there are no noteworthy peaks observed for the 500 fold excess concentration of interference speies. Thus, the RGO/Au-TPP nanocomposite has excellent selectivity for the determination of hydrazine. The stability of the RGO/Au-TPP nanocomposite was characterized by amperometric (*i*-*t*) method. The stability of the modified electrode was investigated from 0 to 3500 sec. The sensor retains 97.6 % of its initial current response after 3500 s of continuous run in 200 μM hydrazine containing PBS (pH 7). The results exhibited that the RGO/Au-TPP nanocomposite has the excellent stability over the 3500 s (Fig. 9B). The practicability of the sensor was demonstrated in ground water sample (Table 2). The found and recovery values are satisfactory and hence RGO/Au-TPP nanocomposite modified electrode has great potential in real-time applications.

4.5 Repeatability, reproducibility and stability studies

Repeatability and reproducibility of the RGO/Au-TPP nanocomposite film modified electrode have been carried out by the cyclic voltammetry in PBS containing 0.1 mM hydrazine.

The proposed sensor exhibited the acceptable level of repeatability with 2.16% relative standard deviation (RSD) for 10 repetitive measurements carried out using single electrode. Moreover, the sensor showed satisfactory reproducibility of 2.98 % for six independent measurements carried out using six independent electrodes. In addition, storage stability of the electrode was monitored. During one month storage period, the modified electrode exhibited stable sensor response towards detection of hydrazine. About, 96.42% of the initial peak current (I_p) was retained after one month of its continuous use which revelaed its excellent storage stability.

5. Conclusions

In summary, we have successfully prepared RGO/Au-TPP nanocomposite through simple and facile electrochemical reduction method and characterized it using NMR, SEM, UV, IR and Raman. The electrochemical studies were carried out by CV and amperometric methods. The RGO/Au-TPP nanocomposite exhibited superior electrocatalytic activity towards detection of hydrazine. The modified electrode shows excellent analytical performance, such as a long linear range from 20 nM to 198 μM and very low detection limit of 3 nM. Furthermore, the sensor possesses high selectivity in the presence of 500 fold excess concentrations of other interfering molecules. The practical applicability of the sensor was verified in various water samples. The sensor had outstanding electrocatalytic activity, sensitivity, stability and reproducibility. Hence, the RGO/Au-TPP nano composite modified electrode as an excellent electrode material for the detection of hydrazine.

Acknowledgement,

This work was supported by the National Science Council and the Ministry of Education, Taiwan (ROC).

References,

1. R. Devasenathipathy, V. Mani, S. M. Chen, D. Arulraj and V. S. Vasantha, *Electrochim. Acta*, 2014, 135, 260-269.
2. S. Palanisamy, B. Thirumalraj and S. M. Chen, *RSC Adv*, 2015, 5, 94591-94598.
3. R. Devasenathipathy, S. Palanisamy, S. M. Chen, C. Karuppiah, V. Mani, S. K. Ramaraj, M. A. Ali and F. M. A. A. Hemaid, *Electroanalysis*, 2015, 27, 1403-1410.
4. Y. You, Y. Yang and Z. Yang, *J. Solid State Electrochem*, 2013, 17, 701-706.
5. J. Li, H. Xie and L. Chen, *Sens. Actuators*, B, 2011, 153, 239-245.
6. C. Wang, L. Zhang, Z. Guo, J. Xu, H. Wang, K. Zhai and X. Zhuo, *Microchim. Acta,* 2010, 169, 1-6.
7. Z. Zhao, Y. Sun, P. Li, S. Sang, W. Zhang, J. Hu and K. Lian, *J. Electrochem. Soc*, 2014, 161, 157-162.
8. Y. Y. Tang, C. L. Kao and P. Y. Chen, *Anal. Chim. Acta*, 2012, 711, 32-39.
9. U. S. Environmental Protection Agency, Integrated risk information system (IRIS) on hydrazine / hydrazine sulfate, National Center for Environmental Assessment, Office of Research and Development, Washington, DC, 1999.
10. W. Zhang, K. H. Y. Jiang, L. Hu, R. H. Chen and P. K. Chu, *Microchim. Acta*, 2011, 175, 137-143.
11. Y. J. Yang, W. Li and X. Wu, *Electrochim. Acta*, 2014, 123, 260-267.
12. M. Sun, L. Bai and D. Q. Liu, *J. Pharm. Biomed. Anal*, 2009, 49, 529-533.
13. F. Dias, A.S. Olojola and B. Jaselskis, *Talanta*, 1979, 26, 47-49.
14. S. Ikeda, H. Satake and Y. Kohri, *Chem. Lett*, 1984, 13, 873-87.
15. M. A. Koupparis and T. P. Hadjiioannou, *Talanta*, 1978, 25, 477-480.
16. C. M. Morenoa, T. Stadler, A. A. Silva, L. C. A. Barbosa and M. E. L. R. Queiroz, *Talanta,* 2012, 89, 369-376.
17. P. V. K. Rao and G. G. Rao, *Talanta*, 1973, 20, 907-910.
18. J. Ding, S. Zhu, T. Zhu, W. Sun, Q. Li, G. Wei and Z. Su, *RSC Adv*, 2015, 5, 22935–22942.
19. X. Li, Z. Chena, Y. Zhong, F. Yanga, J. Pana and Y. Lianga, *Anal. Chim. Acta*, 2012, 710, 118-124.
20. S. H. Wu, F. H. Nie, Q. Z. Chen and J. J. Sun, *Anal. Methods*, 2010, 2, 1729-1736.

21. S. Sakthinathan and S. M. Chen, *Int. J. Electrochem. Sci*, 2015, 10, 6527-6536.
22. R. Madhu, V. Veeramani and S. M. Chen, *Sens. Actuators*, B, 2014, 204, 382-387.
23. S. Sakthinathan, H. F. Lee, S. M. Chen and P. Tamizhdurai, *J. Colloid Interface Sci*, 2016, 468, 120-127.
24. Y. J. Yanga, W. Li and X. Wu, *Electrochim. Acta*, 2014, 123, 260-267.
25. Y. M. Shulga, S. A. Baskakov, V. A. Smirnov, N. Y. Shulga, K. G. Belay and G. L. Gutsev, *J. Power Sources*, 2014, 245, 33-36.
26. F. Y. Tu, T. H. Wu, S. Q. Liu, G. H. Jin and C. Y. Pan, *Electrochim. Acta,* 2013, 106, 406-410.
27. L. Z. Bai, D. L. Zhao, T. M. Zhang, W. G. Xie, J. M. Zhang and Z. M. Shen, *Electrochim. Acta,* 2013, 107, 555-561.
28. H. Dasilva, J. G. Pacheco, J. Mcsmagalhaes, S. Viswanathan and C. Deleruematos, *Biosen. Bioelectron,* 2013, 52, 56-61.
29. H. Wang, D. Sun, N. Zhao, X. Yang, Y. Shi, J. Li, Z. Su and G. Wei, *J. Mater. Chem. B*, 2014, 2, 1362-1370.
30. X. Wang, L. Zhi and K. Mullen, *Nano Lett*, 2007, 8, 323–327.
31. G. Wei, Y. Zhang, S. Steckbeck, Z. Su and Z. Li, *J. Mater. Chem*, 2012, 22, 17190-17195.
32. W. Chen, L. Yan and P. R. Bangal, *Carbon*, 2010, 48, 1146-1152.
33. W. Chen, L. Yan and P. R. Bangal, *J. Phys. Chem. C*, 2010, 114, 19885–19890.
34. M. A. Raj and S. A. John, *J. Phys. Chem. C*, 2013, 117, 4326−4335.
35. Z. Xiong, Z. D. Cheng, C. Yao, S. X. Zhong and M. A. Y. Wei, *Chin. Sci. Bull*, 2012, 57, 3045-3050.
36. J. F. V. Staden and R. I. S. Staden, *Talanta*, 2010, 80, 1598-1605.
37. M. Biesaga, K. Pyrzynska and M. Trojanowicz, *Talanta*, 2000, 51, 209-224.
38. A. J. Gross, C. Bucher, L. C. Guerente, P. Labbé , A. J. Downard and J. C. Moutet, *Electrochem. Commun*, 2011, 13, 1236-1239.
39. P. Muthukumar and S. A. John, *J. Solid State Electrochem*, 2014, 18, 2393-2400.
40. L. Zheng, D. Ye, L. Xiong, J. Xu, K. Tao, Z. Zou, D. Huang, X. Kang, S. Yang and J. Xia, *Anal. Chim. Acta*, 2013, 768, 69-75.
41. A. Nijamudheen, D. Jose and A. Datta, *J. Phys. Chem. C*, 2011, 115, 2187-2195.

42. M. P. Eng, T. Ljungdahl, J. Andreasson, J. Martensson and B. Albinsson, *J. Phys. Chem. A*, 2005, 109, 1776-1784.
43. Y. F. To, R. W. Sun, Y. Chen, V. S. F. Chan, W. Y. Yu, P. K. H. Tam, C. M. Che and C. L. S. Lin, *Int. J. Cancer*, 2009, 124, 1971–1979.
44. A. D Adler, F. R. Longo, J. D. Finarelli, J. Goldmacher, J. Assour and L. Korsakoff, *J. Org. Chem,* 1967, 32, 476-476.
45. C. M. Che, R. W. Y. Sun, W. Y. Yu, C. B. Ko, N. Zhu and H. Sun, *Chem. Commun*, 2003, 14,1718-1719.
46. E. B. Fleischer and A. Laszlo, *Inorg. Nucl.Chem. Letters,* 1969, 5, 373-376.
47. W. S. Hummers and R. E. Offeman, *J. Am. Chem. Soc*, 1958, 80, 1339-1339.
48. G. Chottard, P. Battioni, J. P. Battioni, M. Lange and D. Manusu, *Inorg. Chem*, 1981, 20, 1718-1722.
49. K. Deng, J. Zhou and X. Li, *Electrochim. Acta*, 2013, 114, 341-346.
50. S. Eigler, C. Dotzer and A. Hirsch, *Carbon*, 2012, 50, 3666 -3673.
51. N. Li, M. Zhu, M. Qu, X. Gao, X. Li, W. Zhang, J. Zhang and J. Ye, *J. Electroanal. Chem*, 2011, 651, 12-18.
52. A. J. Bard and L. R. Faulkner, Electrochemical methods fundamentals and applications, Wiley, New York, 2001.
53. C. Y. Lin, A. Balamurugan, Y.H. Lai and K.C. Ho, *Talanta*, 2010, 82, 1905-1911.
54. R. Madhu, B. Dinesh, S. M. Chen, R. Saraswathi and V. Mani, *RSC Adv*, 2015, 5, 54379–54386.
55. S. V. Guerra, C. R. Xavier, S. Nakagaki and L. T. Kubota*, Electroanalysis*, 1998, 10, 462-466.
56. H. R. Zare and N. Nasirizadeh, *Electrochim. Acta*, 2007, 52, 4153-4160.
57. Y. Liu, Y. Li and X. He, *Anal. Chim. Acta*, 2014, 819, 26-33.
58. S. Mutyala and J. Mathiyarasu, *Sens. Actuators, B*, 2015, 210, 692-699.
59. H. R. Zare, Z. Sobhani and M. M. Ardakani, *J.Solid State Electrochem,* 2007, 11, 971-979.
60. S. Dutta, C. Ray, S. Mallick, S. Sarkar, A. Roy and T. Pal, *RSC Adv,* 2015, 5, 51690–51700.

61. R. Devasenathipathy, S. H. Tsai, S. M. Chen, C. Karuppiah, R. Karthik and S. F. Wang, *Electroanalysis*, 2016, 28, 1-8.

Figure caption,

Table 1 Combarision of the analytical performance of RGO/Au-TPP nanocomposite modified electrode with the other reported sensor.

Table 2 Determination of hydrazine for real sample analysis in various water samples using RGO/Au-TPP nanocomposite modified electrode.

Scheme 1 Synthesis of Gold Tetra Phenyl porphyrin (Au-TPP).

Scheme 2 Schematic representation for the preparation of RGO/Au-TPP nanocomposite modified electrode for hydrazine sensor.

Figure 1 SEM images of (A) GO, (B) RGO, (C) GO/Au-TPP and (D) RGO/Au-TPP, (Inset C') Au-TPP, **(E)** EDX spectrum of RGO/Au-TPP nanocomposite.

Figure 2 TEM image of (A) RGO, (B) AuTPP, (C) (D) RGO/Au-TPP nanocomposite.

Figure 3A) Raman spectra of (a) RGO, (b) AuTPP and (c) RGO/Au-TPP nanocomposite, **Figure 3B** FT-IR spectra of (a) RGO, (b) Au-TPP and (c) RGO/Au-TPP nanocomposite.

Figure 4A) UV-Vis spectroscopy analysis of (a) GO, (b) RGO, (c) Au-TPP, (d) RGO/Au-TPP, **Inset** (a') GO and (b') RGO. **4B)** Electrochemical impedance spectra of (a) bare GCE, (b) GO, (c) Au-TPP, (d) RGO and (e) RGO/Au-TPP modified electrode in 0.1 M KCl containing 5 mM $[Fe(CN)_6]^{3-/4-}$.

Figure 5A) Cyclic voltammograms of (a) bare GCE, (b) GO, (d) RGO, (e) Au-TPP, (f) GO/Au-TPP and (g) RGO/Au-TPP nanocomposite modified electrode PBS (pH7) containing 200 µM hydrazine at the scan rate 50 mVs^{-1}, (c) RGO/Au-TPP without hydrazine.

Figure 5B) Cyclic voltammogram of RGO/Au-TPP nanocomposite in 0.05 M PBS (pH 7) containing different concentrations of hydrazine at scan rate (50 mV s^{-1}).

Figure 6A) Cyclic voltammograms of RGO/Au-TPP nanocomposite modified GCE in PBS (pH 7) containing 200 μM hydrazine containing different pH (3, 5, 7, 9 and 11). **6B)** calibration plot for pH vs I_p. **6C)** pH vs E_P (V).

Figure 7A) Cyclic voltammetry response of the RGO/Au-TPP nanocomposite modified GCE in PBS containing 200 μM of hydrazine at different scan rate. **(B)** calibration plot of square root of scan rate vs. peak current. (**C)** calibration plot of the logarithm of scan rate vs. peak current.

Figure 8A) Amperometric response for the different concentrations of hydrazine in PBS (pH 7). E_{app} = 0.16 V. Inset: peak current vs [hydrazine].

Figure 9A) Selectivity: Amperometric response of hydrazine at RGO/Au-TPP nanocomposite modified electrode in presence of common interference ions, E_{app} = 0.16 V.

Figure 9B) Stability studies of RGO/Au-TPP nanocomposite modified electrode.

Table 1 Combarision of the analytical performance of RGO/Au-TPP nanocomposite modified electrode with the other reported sensor.

Modified electrodes	Linear range/μM	LOD[a] (nM)	Sensitivity/ $\mu A \mu M^{-1} cm^{-2}$	Ref.
MWCNT[b] / FeTsPc[c].	0.1-3	7.6	–	4
ZnO-Msp[d] /AuNp[e]	0.05-5	18	5.54	54
Cu-TPP[g]/ Zeolite	0.2-1	100	–	55
Hematoxylin /MWCNT	2.0-122.8	680	0.020	56
Zinc Oxide / RGO Nc	1.0-33.5	800	–	18
CeNps[h]/mesoporous electrode	0.04-192	12	0.147	57
GNF[i]/GCE	0.5-7.5	300	0.028	58
Rutin / MWCNT / GCE[f]	2.0-190.0	610	0.065	59
Au@Pd[j]/RGO	2-40	0.08	11.8	60
RGO/β-CD[k]/AgNPs[l]	0.08-1110	1.4	1.584	61
RGO[m]/Au-TPP Nc[n]	0.02-198	5	2.266	This work

[a]Limit of Detection, [b]Multiwalled carbon nanotubes, [c]Iron Tetra sulfonate Phthalocyanine, [d]Zing oxide microsphere, [e]Gold nanoparticle, [f]Glassy carbon electrode, [g]Copper tetra phenyl porphyrin, [h]Cerium nanoparticle, [i]graphene nano flake, [j]Gold and palladium nanocluster, [k]β-Cyclodextrin [l]Gold nano aprticles, [m]Reduced graphene oxide Gold, [n]Gold tetraphenyl porphyrin nanocomposite.

Table 2 Determination of hydrazine in water samples using RGO/Au-TPP/GCE

Samples	**Added/μM**	**Found/μM**	**Recovery/%**	***RSD/%**
1. Ground water sample	100	104.3	104.3	3.5
	200	202.2	101.1	3.3
2. Rain water sample	100	99.5	99.5	2.7
	200	199.4	99.7	2.8
3. River water sample	100	102.3	102.3	3.3
	200	199.3	99.6	3.0

*Relative standard deviation of 3 individual measurements.

Scheme1,

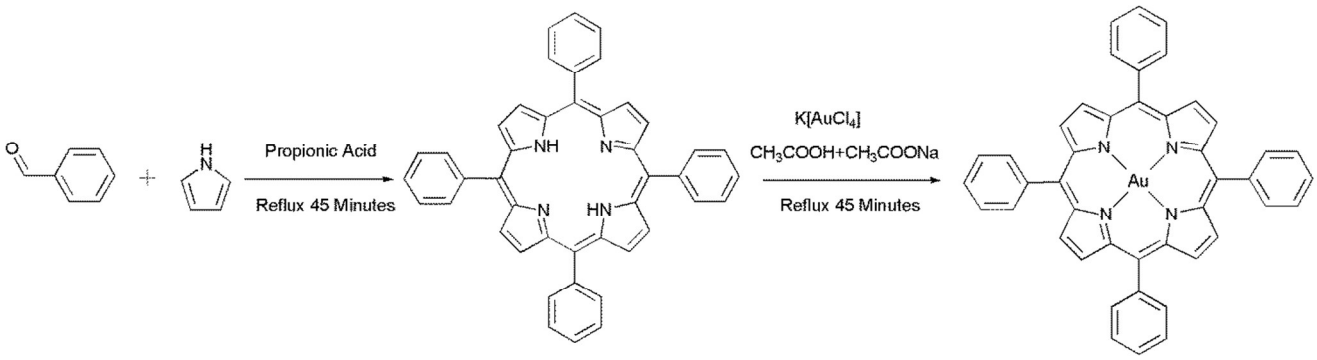

Scheme 2,

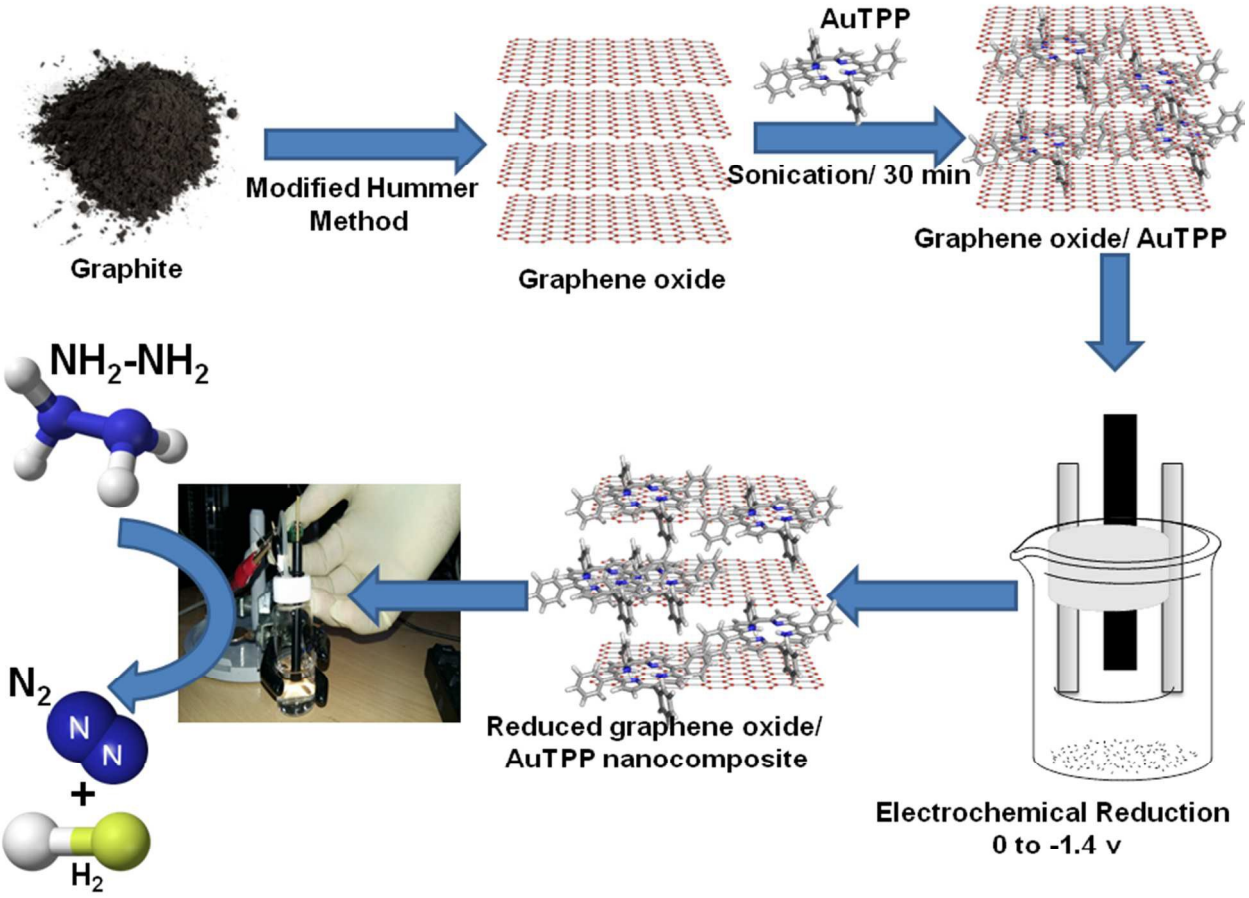

Figure 1,

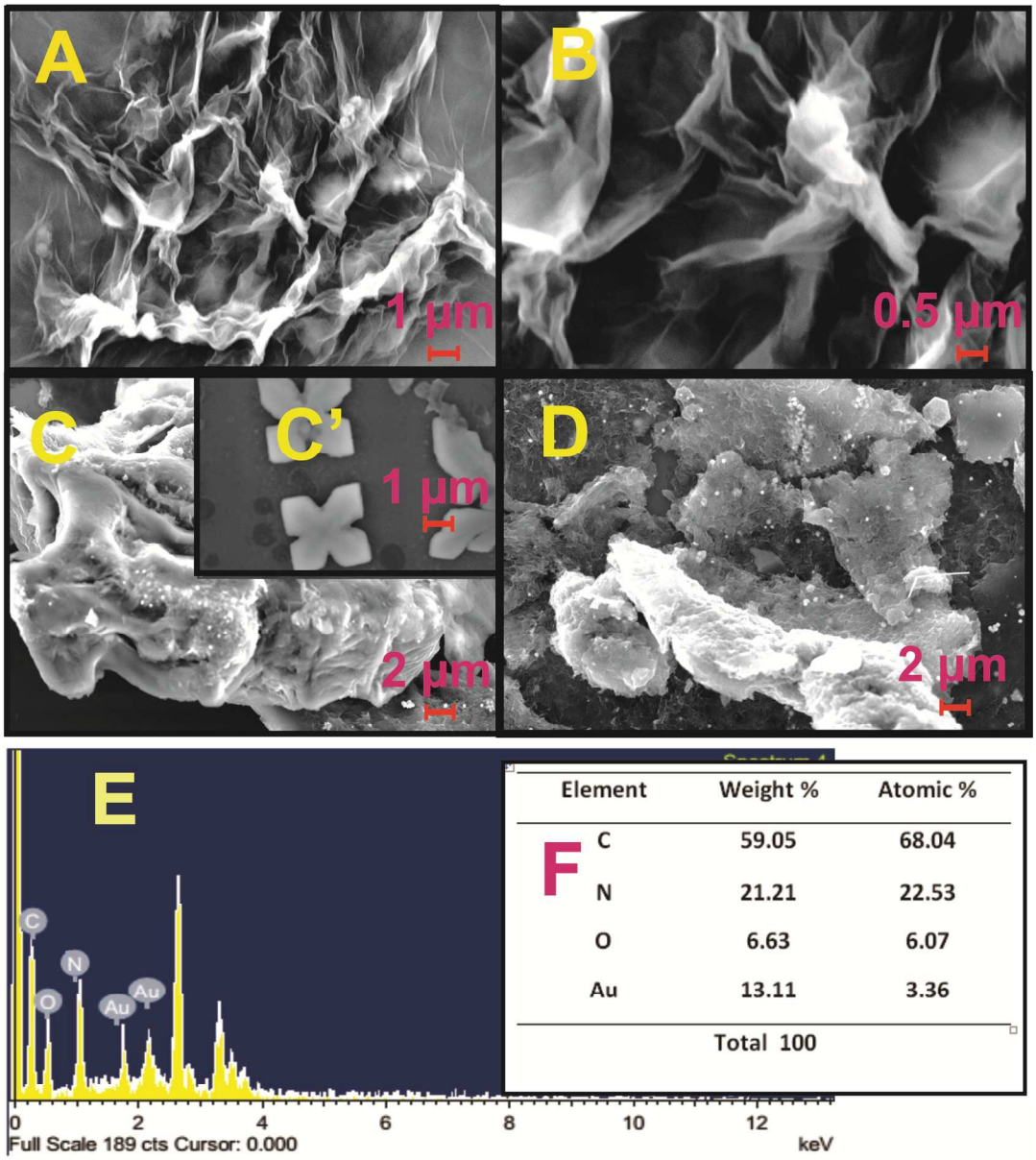

Figure 2,

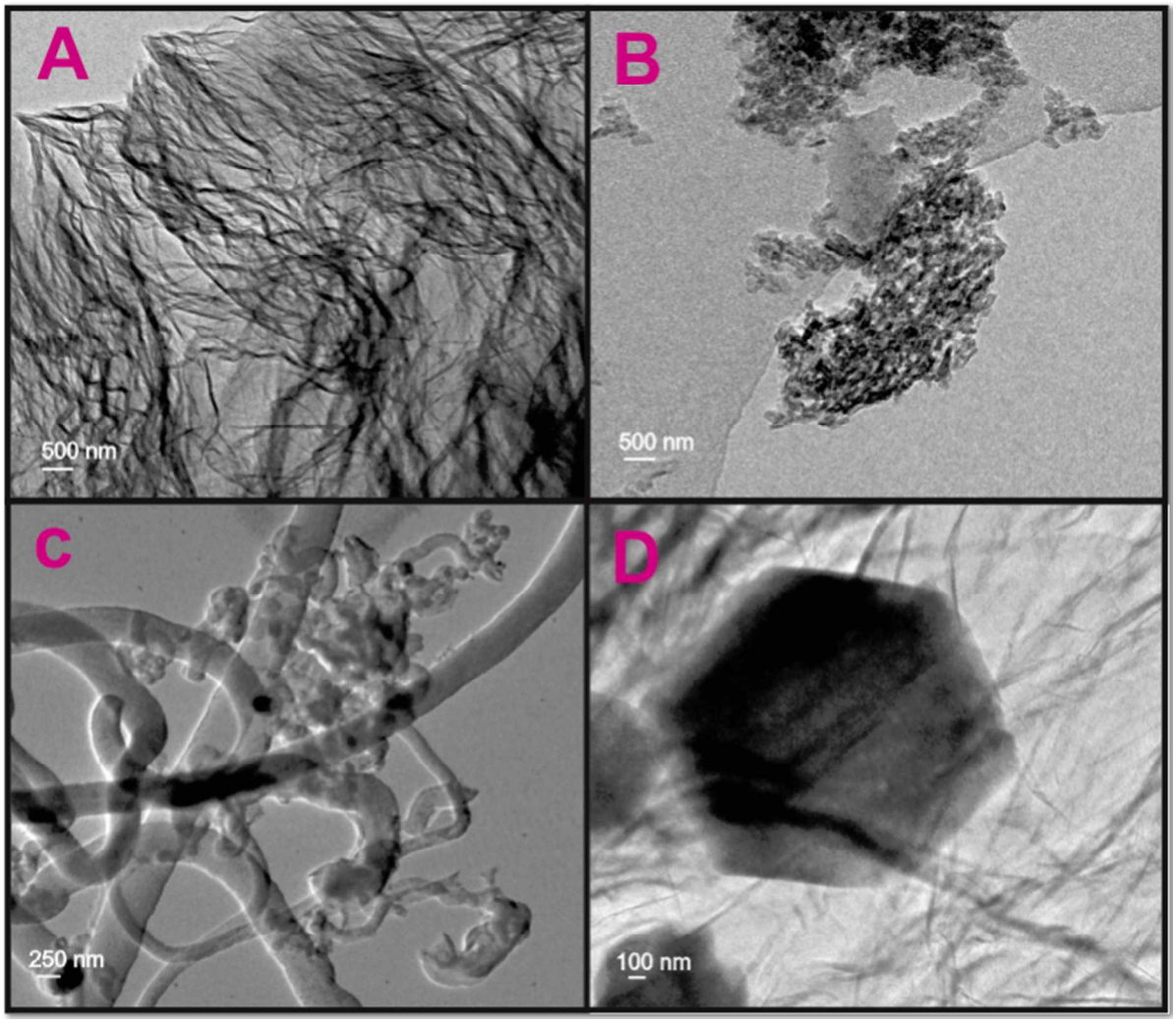

Figure 3,

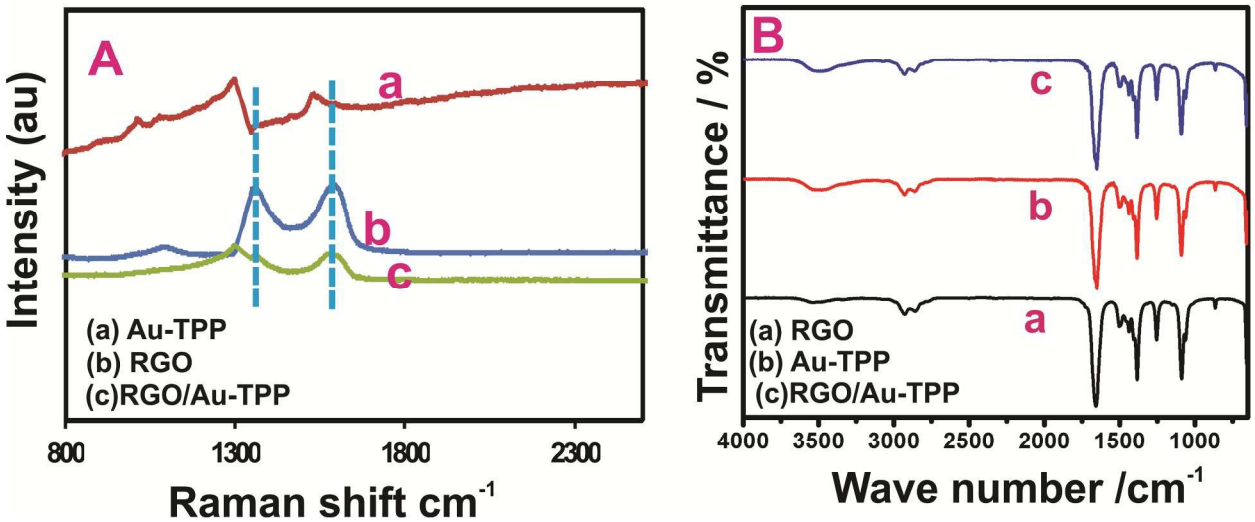

Figure 4,

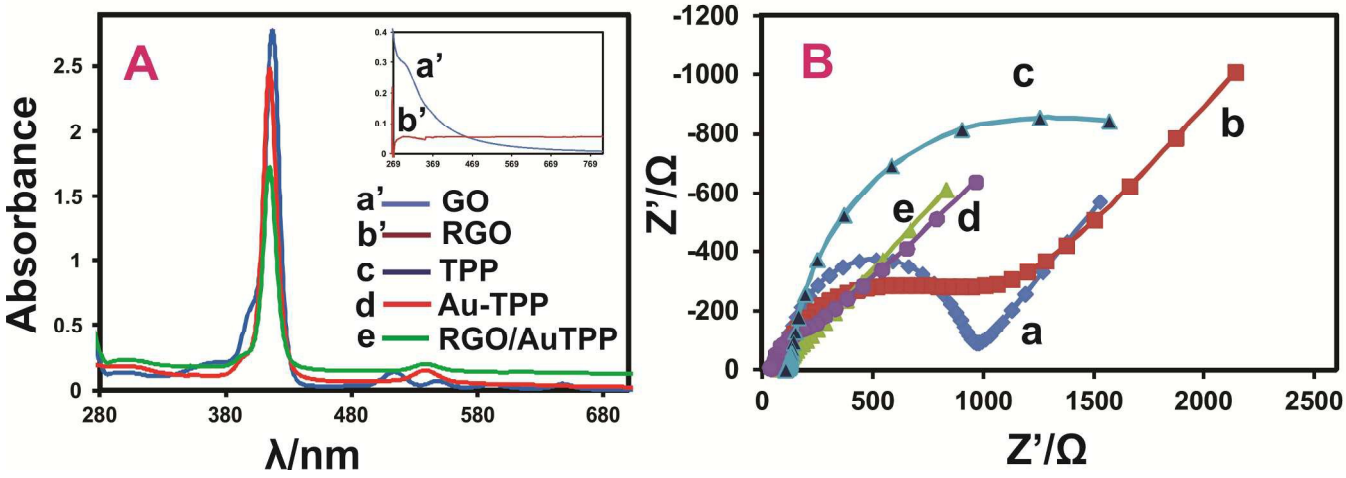

Figure 5,

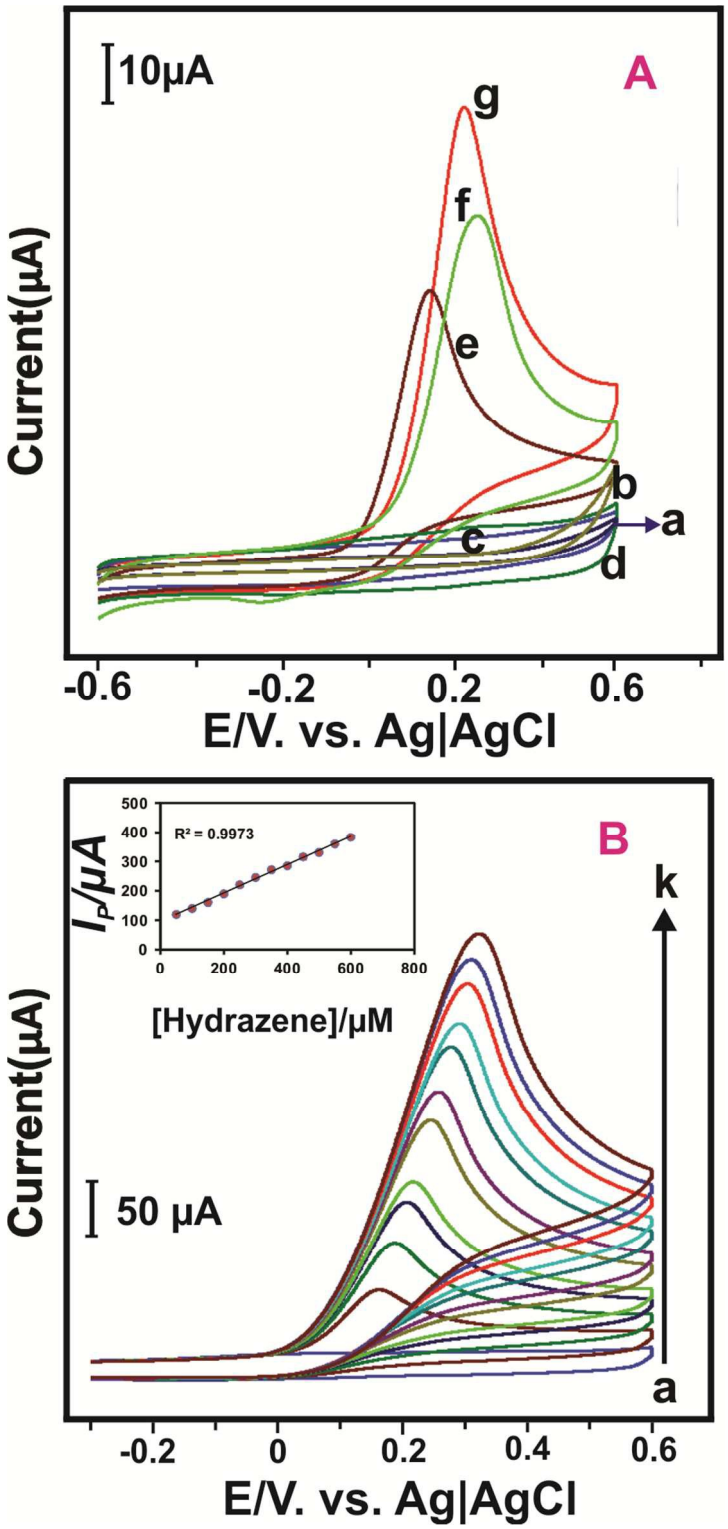

Figure 6,

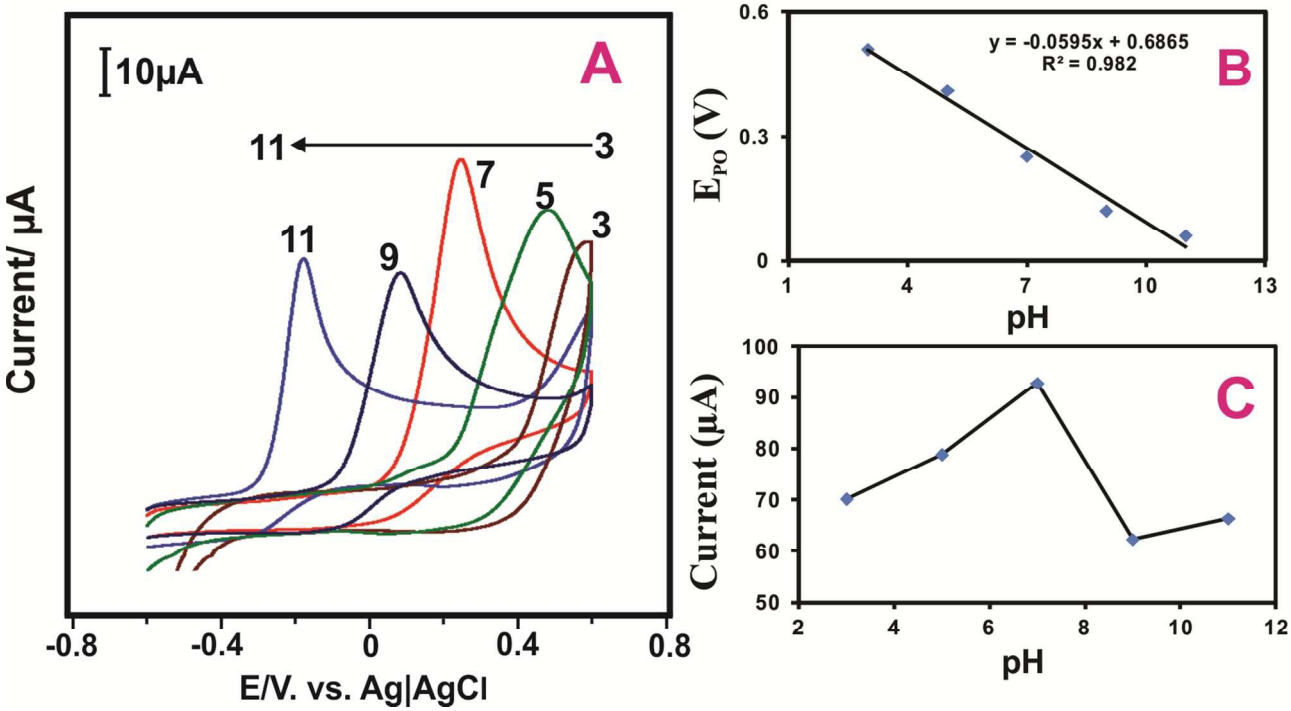

Figure 7,

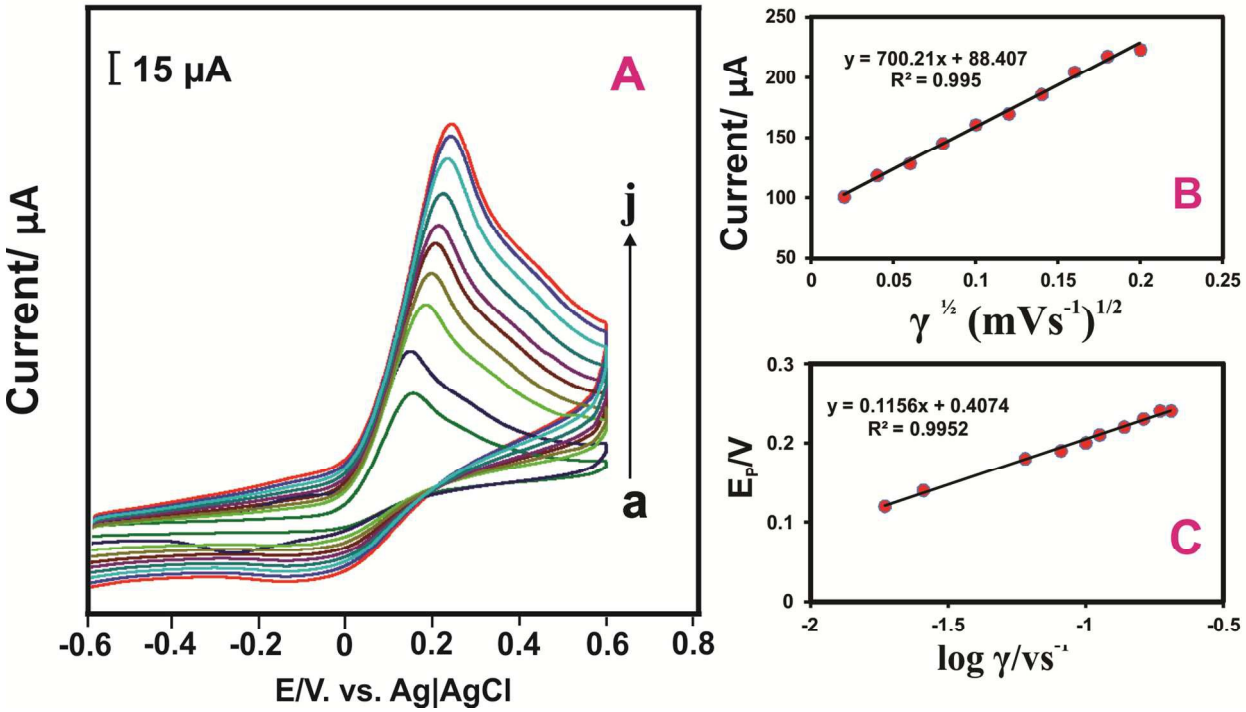

Figure 8,

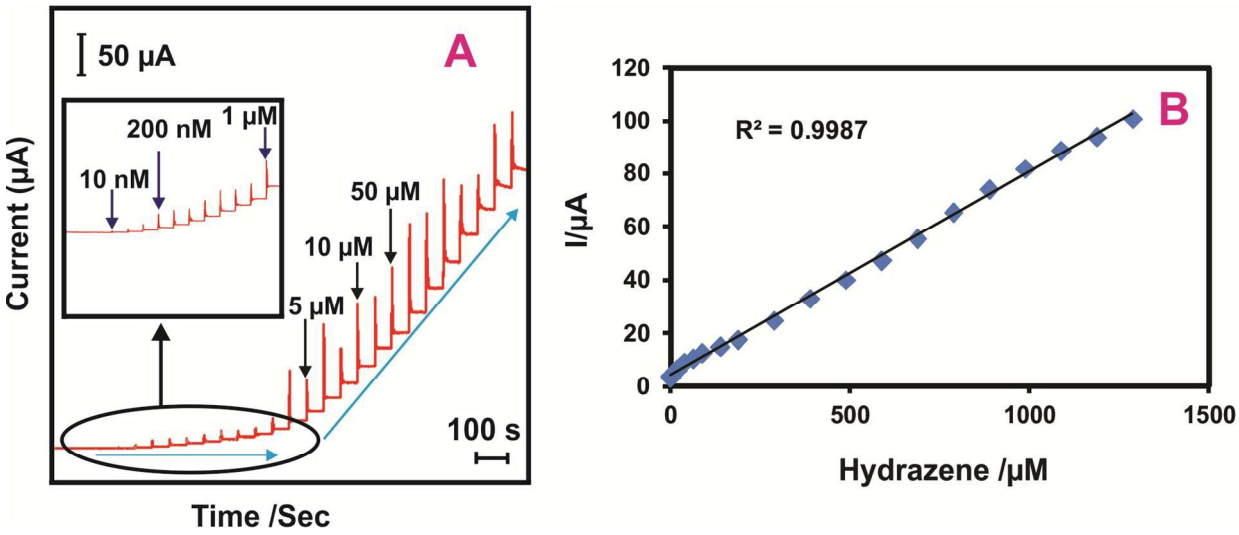

Figure 9,

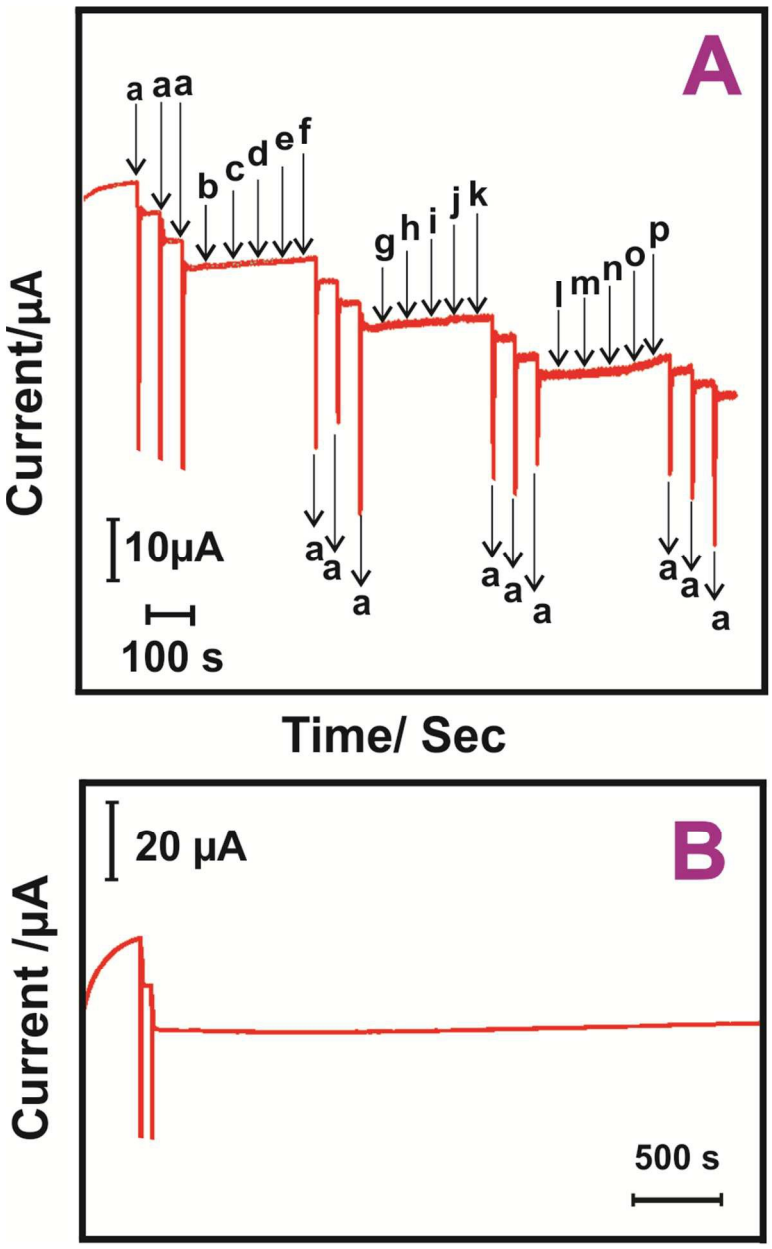

Graphical abstract,